Electronic Supplementary Information

Boosting photocatalytic H_2 generation by assembling copper complex and carbon nanotubes onto carbon nitride polymer

Jun-Shuai Zhang[a, b], Wen-Chen Zhou[a], Jia-Yu Lai[a], Wei-De Zhang[a*]

[a]*School of Chemistry and Chemical Engineering, South China University of Technology, 381 Wushan Road, Guangzhou 510640, People's Republic of China*

[b]*School of Material Science and Technology, Jinan University, Jinan, Shandong 250022, People's Republic of China*

[*]Corresponding author. Tel and Fax: 86-20-8711 4099, E-mail address: zhangwd@scut.edu.cn (W. D. Zhang).

Materials

Urea (AR), $NaHCO_3$ (AR) and NaCl (AR) were obtained from Guangdong Guanghua Sci- Tech Co., Ltd (Guangzhou, China). N, N-dimethylformamide (DMF, 99.5%), concentrated hydrochloric acid (HCl, 36-38%) and diethyl ether were purchased from Guangzhou Chemical Reagent Factory (Guangzhou, China). Triethanolamine (TEOA, 98.0%), paraformaldehyde (AR), salicylaldehyde (AR, 98%), diaminomaleoniltrile (TCNQ,⩾96.0%) and $CuCl_2 \cdot 2H_2O$ (AR) were purchased from Aladdin Chemistry Co. Ltd. (Shanghai, China). CNTs (20-30 nm) were purchased from XF Nano Technology Co. Ltd. (Nanjing, China). All reagents in this work were acquired from commercial sources and used without further purification. The deionized (DI) water was produced from Pure Water System (GWA-UN, Beijing, China).

Synthesis of 5-Chloromethyl-2-hydroxybenzaldehyde

5-Chloromethyl-2-hydroxybenzaldehyde was prepared according to the previous report [1]. In a 100 mL two-necked flask, paraformaldehyde (5.0 g, 167 mmol), salicylaldehyde (10.0 g, 82 mmol), and 50 mL of concentrated hydrochloric acid were mixed under rapid stirring. After reaction for 48 h at room temperature, the mixture was diluted and filtered, then the solid product was dissolved in diethyl ether and extracted with water, saturated $NaHCO_3$, and NaCl solution successively. After evaporation of the solvent, the crude product was recrystallized with petroleum ether (60-90 °C), and the white final product was obtained.

Characterization

Fourier transform infrared (FT-IR) spectra were detected in a range of 400-4000 $cm^{-1}$with a resolution of 4 cm^{-1} by using an IR Affiniy-1 FTIR spectrometer. The chemical state of photocatalysts were examined by X-ray photoelectron spectroscopy (XPS, Thermo ESCALAB 250XI, USA). X-ray diffractometer (XRD) is applied to characterize the phase composition and crystal structures of hybrids on Bruker GADDS diffractometer with a Cu Kα source. The morphologies and structures of typical samples were observed by the scanning electron microscope (SEM merlin) and transmission electron microscopy (TEM, JEM-2100F). The UV-vis diffuse reflectance spectra (UV-vis DRS) were tested by Hitachi U-3010 using $BaSO_4$ as the standard reference with an integrating sphere scanning from 200 to 800 nm. Hitachi F-4500 fluorescence spectrophotometer was utilized to monitor the photoluminescence (PL) spectra of samples. The copper contents of samples were analyzed by inductively coupled plasma spectrometer (ICP-OES, PerkinElmer Optima 8300).

DFT calculation

DFT calculations were performed using Gaussian 09 program to simulate the HOMO and LUMO electron distribution of CN and CuL/CN. All calculations utilized a B3LYP function and 6-31 G (d, p) basis set. The DFT calculation can only interpret the experimental observations qualitatively. Therefore, the minimum trimmer unit cell with a pore is chosen as the calculation model. The structural optimizations were carried out without any symmetry constraints.

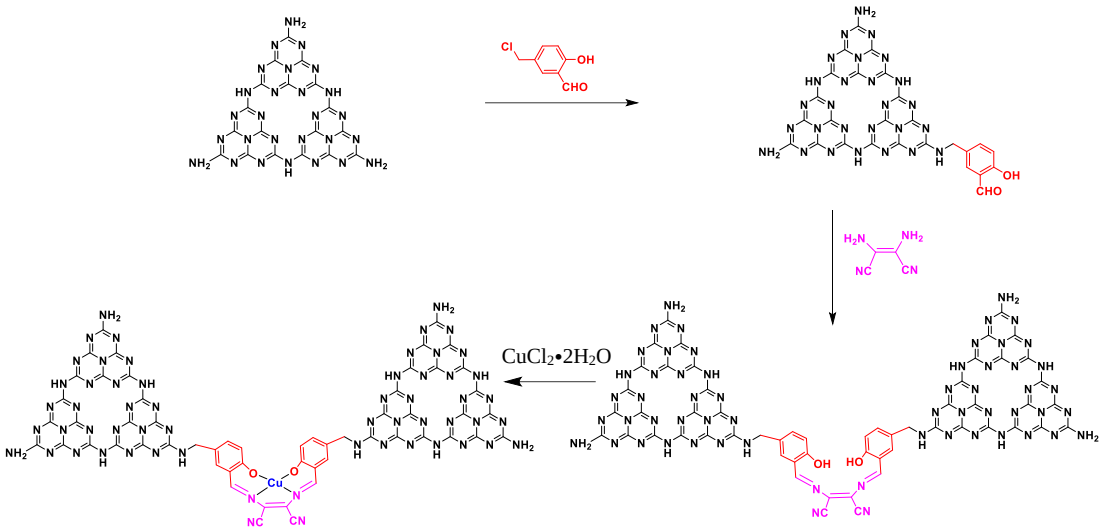

Figure S1. Synthesis route of CuL/CN.

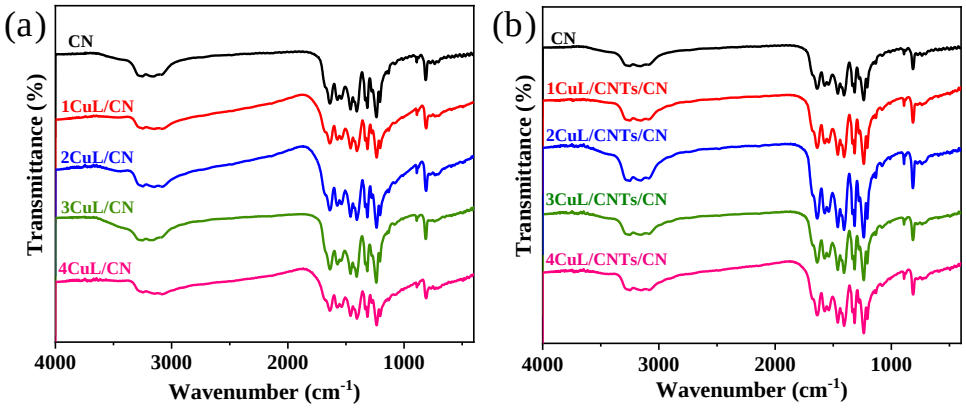

Figure S2. FT-IR spectra of the obtained catalysts.

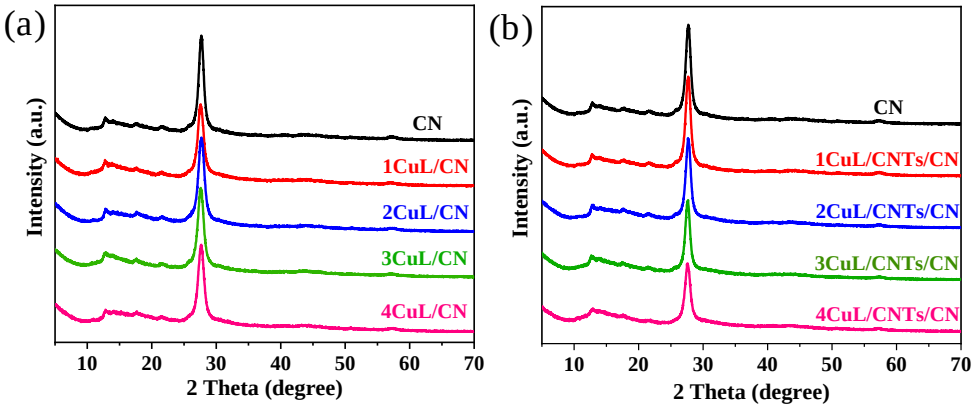

Figure S3. XRD patterns of the prepared catalysts.

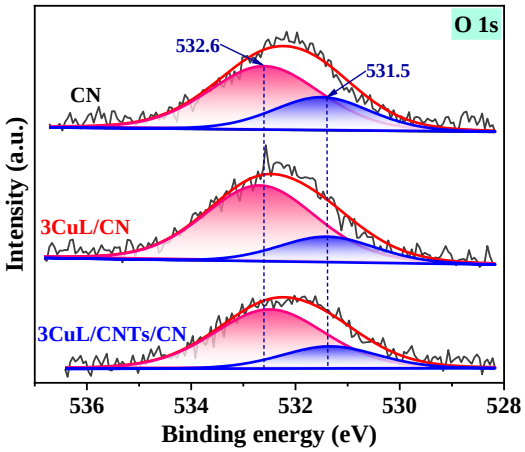

Figure S4. High-resolution XPS spectra of O 1s of CN, 3CuL/CN and 3CuL/CNTs/CN.

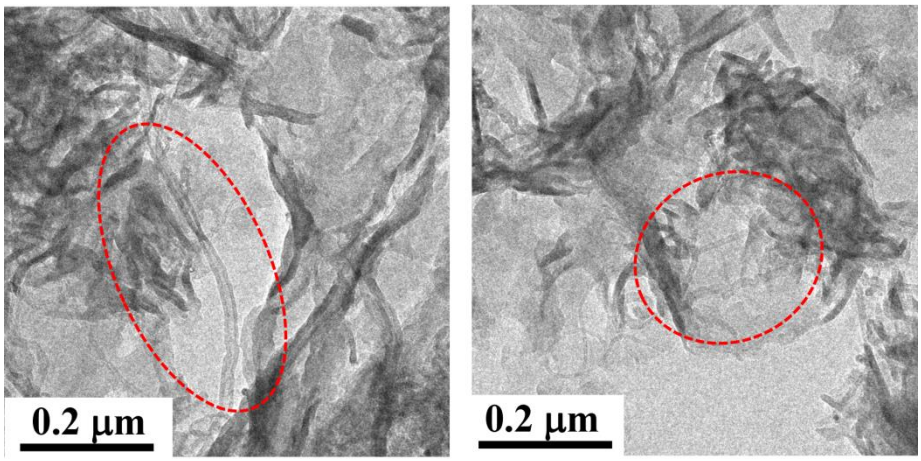

Figure S5. The magnified TEM images of 3CuL/CNTs/CN.

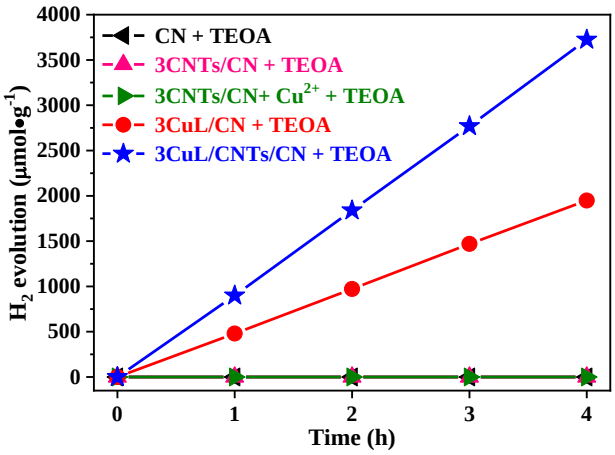

Figure S6. Photocatalytic H_2 production on CN-based hybrids under different conditions.

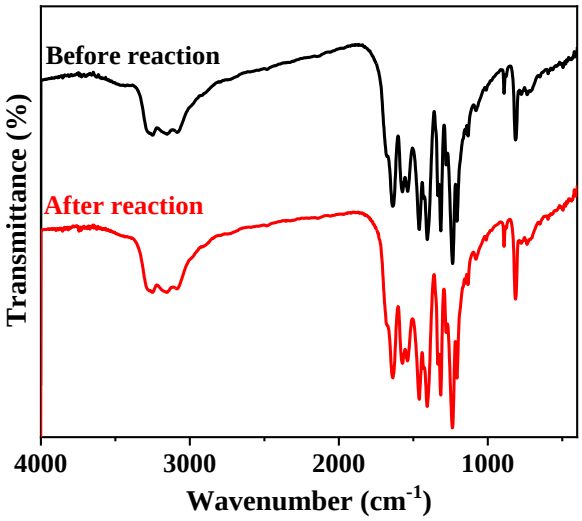

Figure S7. FT-IR spectra of 3CuL/CNTs/CN before and after photocatalytic reaction.

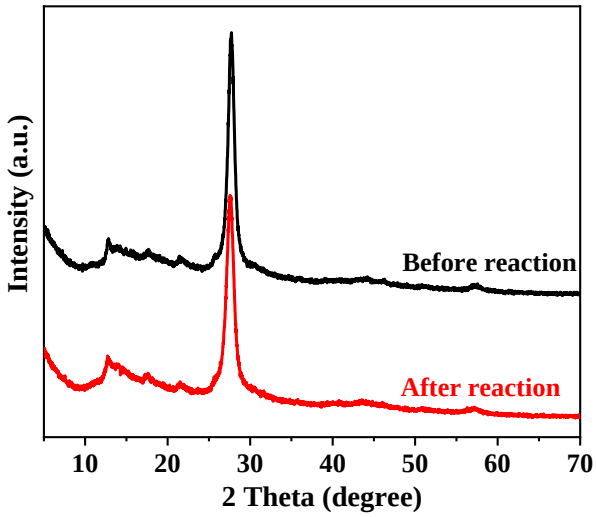

Figure S8. XRD patterns of 3CuL/CNTs/CN before and after photocatalytic reaction.

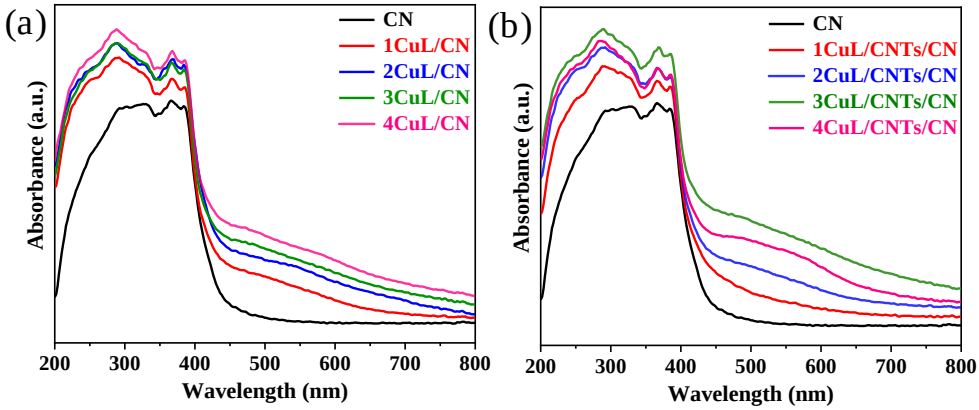

Figure S9. UV spectra of the obtained samples.

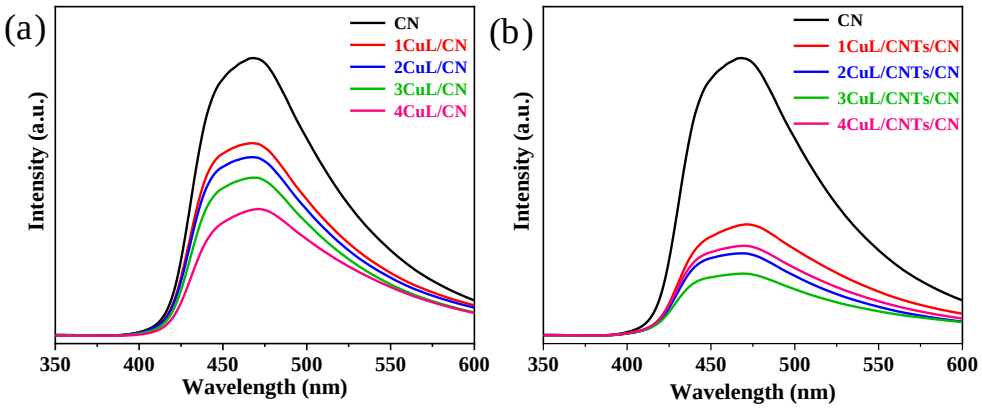

Figure S10. PL spectra of the samples.

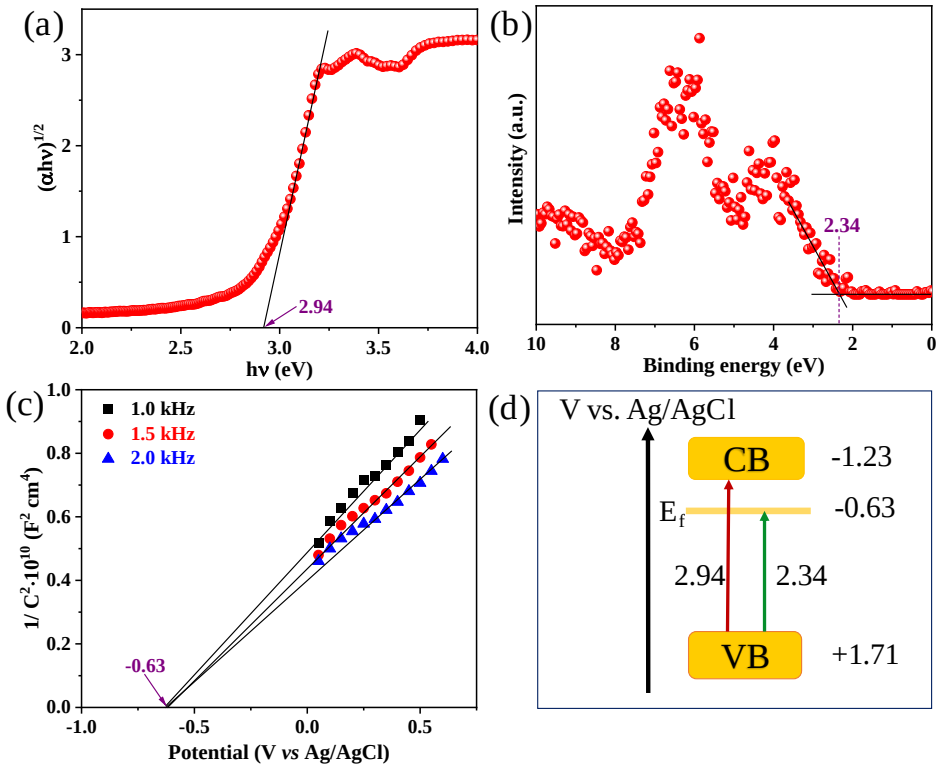

Figure S11. (a) The bandgap, (b) VB-XPS, (c) MS curves, and (d) band position (*vs.* Ag/AgCl) of the prepared CN.

Table S1. Elemental compositions (atom ratios) of the samples detected by XPS.

Sample	C (at%)	N (at%)	O (at%)	Cu (at%)	C/N
CN	42.31	54.09	3.60	0	0.78
3CuL/CN	44.14	51.22	4.34	0.30	0.86
3CuL/CNTs/CN	44.68	51.61	3.39	0.31	0.87

Table S2. Relative ratios of carbon species from C 1s spectra for CN and 3CuL/CN.

Sample	N-C=N		C=C		C-N	
	B. E. (eV)	%	B. E. (eV)	%	B. E. (eV)	%
CN	288.2	90.97	284.8	9.03	-	-
3CuL/CN	288.3	86.08	284.8	10.45	286.3	3.47
3CuL/CNTs/CN	288.3	82.97	284.8	12.19	286.3	4.84

Table S3. Relative ratios of nitrogen species from high-resolution XPS spectra of N 1s spectra for CN, 3CuL/CN and 3CuL/CNTs/CN.

Sample	C-NH		C-N=C		N-$(C)_3$		π excitations	
	B. E. (eV)	%	B. E. (eV)	%	B. E. (eV)	%	B. E. (eV)	%
CN	401.0	15.01	398.7	55.35	399.5	24.16	404.5	5.48
3CuL/CN	401.2	13.94	398.8	55.53	399.6	25.40	404.5	5.13
3CuL/CNTs/CN	401.1	14.61	398.8	55.78	399.6	24.07	404.5	5.54

Table S4. Comparison of the Cu elemental contents in 3CuL/CN and 3CuL/CNTs/CN according to ICP-OES.

Sample	Cu dosage (wt%)	Cu content (wt%)
CN	0	0
3CuL/CN	1.86	0.236
3CuL/CNTs/CN	1.86	0.242

Table S5 Comparison of photocatalytic H_2 evolution performance over the recently reported g-C_3N_4 catalysts modified with non-noble metal based cocatalysts.

Catalyst	Light intensity ($mW \cdot cm^{-2}$)	Sacrificial reagent	H_2 Evolution Rate ($\mu mol\ h^{-1}\ g^{-1}$)	Ref.
EY/Ni-Cu/g-C_3N_4	-	TEOA	2088	[2]
3CuL/CNTs/CN	100	TEOA	931.0	*This work*
2D-Ni_2P@BP/CN	100	TEOA	858.2	[3]
Cu/g-C_3N_4	-	TEOA	470.0	[4]
7wt% Cu-Cu_2O/g-C_3N_4	150	TEOA	400.0	[5]
CN-0.5 wt% AB-2% CuS	-	TEOA	348.0	[6]
Ni_3N/g-C_3N_4	-	TEOA	305.0	[7]
1.0 wt% Cu_3P-FCN	-	TEOA	277.2	[8]
Cu@C/g-C_3N_4	-	TEOA	275.0	[9]
NiS_2/g-C_3N_4	-	TEOA	239.0	[10]
CoP/g-C_3N_4	-	TEOA	201.5	[11]
0D/2D FeP/g-C_3N_4	-	TEOA	178	[12]
1.0 wt% Cu_3P/ g-C_3N_4	-	TEOA	159.4	[13]
$Ni(OH)_2$–g-C_3N_4	-	TEOA	152.0	[14]
FL dye/g-C_3N_4/$Cu_2(OH)_2CO_3$	-	TEOA	22.6	[15]

References

[1] Z. Li, S. Wu, D. Zheng, J. Liu, H. Liu, H. Lu, Q. Huo, J. Guan and Q. Kan, *Appl. Organomet. Chem.*, 2014, **28**, 317–323.

[2] Z. L. Jin and L. J. Zhang, *J. Mater. Sci. Technol.*, 2020, **49**, 144–156.

[3] R. Boppella, W. S. Yang, J. W. Tan, H. C. Kwon, J. Park and J. Moon, *Appl. Catal. B Environ.*, 2019, **242**, 422–430.

[4] P. Y. Zhang, T. Song, T. T. Wang and H. P. Zeng, *Int. J. Hydrog. Energy*, 2017, **42**,

14511–14521.

[5] P. Y. Zhang, T. T. Wang and H. P. Zeng, *Appl. Surf. Sci.*, 2017, **391**, 404–414.

[6] R. C. Shen, J. Xie, P. Y. Guo, L. S. Chen, X. B. Chen and X. Li, *ACS Appl. Energy Mater.*, 2018, **1**, 2232–2241.

[7] J. H. Ge, Y. J. Liu, D. C. Jiang, L. Zhang and P. W. Du, *Chinese J. Catal.*, 2019, **40**, 160–167.

[8] R. C. Shen, J. Xie, X. Y. Lu, X. B. Chen and X. Li, *ACS Sustainable Chem. Eng.*, 2018, **6**, 4026–4036.

[9] S. B. Chen, S.Y. Yang, X. L. Sun, K. L. He, Y. H. Ng, X. Cai, W. Y. Zhou and Y. P. Fang, *Energy Technol.*, 2019, **7**, 1800846.

[10] H. T. Li, M. Wang, Y. P. Wei and F. Long, *J. Colloid Interf. Sci.*, 2019, **534**, 343–349.

[11] X. J. Sun, D. D. Yang, H. Dong, X. B. Meng, J. L. Sheng, X. Zhang, J. Z. Wei and F. M. Zhang, *Sustain. Energ. Fuels*, 2018, **2**, 1356–1361.

[12] H. C. Yang, R. Y. Cao, P. X. Sun, X. L. Deng, S. W. Zhang and X. J. Xu, *Appl. Surf. Sci.*, 2018, **458**, 893–902.

[13] W. C. Wang, X. L. Zhao, Y. N. Cao, Z. P. Yan, R. X. Zhu, Y. Tao, X. L. Chen, D. Q. Zhang, G. S. Li and D. L. Phillips, *ACS Appl. Mater. Interfaces*, 2019, **11**, 16527–16537.

[14] J. G. Yu, S. H. Wang, B. Cheng, Z. Lin and F. Huang, *Catal. Sci. Technol.*, 2013, **3**, 1782–1789.

[15] Y. M. Liu, X. X. Wu, H. Lv, Y. F. Cao and H. Ren, *Dalton Trans.*, 2019, **48**, 1217-

1225.